Net ecosystem exchange over heterogeneous Arctic tundra: Scaling between chamber and eddy covariance measurements

Net ecosystem exchange over heterogeneous Arctic tundra: Scaling between chamber and eddy covariance measurements

Andrew M. Fox,[1,2] Brian Huntley,[1] Colin R. Lloyd,[3] Mathew Williams,[4] and Robert Baxter[1]

Received 4 June 2007; revised 3 March 2008; accepted 6 March 2008; published 20 June 2008.

[1] Net ecosystem exchange (NEE) was estimated for an area of tundra near Abisko using both eddy covariance (EC) data and chamber measurements. This area of tundra is heterogeneous with six principal elements forming a landscape mosaic. Chamber measurements in patches of the individual mosaic elements were used to model NEE as a function of irradiance and temperature. The area around the EC mast was mapped, and a footprint model was used to simulate the varying source fraction attributable to each mosaic element. Various upscaling approaches were used to estimate NEE for comparison with NEE calculated from the EC observations. The results showed that EC measurements made for such a heterogeneous site are robust to the variations in NEE between mosaic elements that also vary substantially in their source fractions. However, they also revealed a large (~60%) bias in the absolute magnitude of the cumulative negative NEE for a 40-day study period simulated by various upscaling approaches when compared to the value calculated from the EC observations. The magnitude of this bias, if applied to estimates for the entire tundra region, is substantial in relation to other components of the global carbon budget. Various hypotheses to account for this bias are discussed and, where possible, evaluated. A need is identified for more systematic sampling strategies when performing chamber measurements in order to assess the extent to which subjectivity of chamber location may account for much of the observed bias. If this is the origin of the bias, then upscaling approaches using chamber measurements may generally overestimate CO_2 uptake.

Citation: Fox, A. M., B. Huntley, C. R. Lloyd, M. Williams, and R. Baxter (2008), Net ecosystem exchange over heterogeneous Arctic tundra: Scaling between chamber and eddy covariance measurements, *Global Biogeochem. Cycles*, *22*, GB2027, doi:10.1029/2007GB003027.

1. Introduction

[2] Climatic changes projected as a consequence of human perturbation of the global carbon cycle [*Cubasch et al.*, 2001; *Intergovernmental Panel on Climate Change* (*IPCC*), 2001, 2007] have stimulated much recent research that aims to quantify components of the natural carbon cycle. Many of these studies have focused upon quantifying land surface–atmosphere fluxes of the primary naturally occurring radiatively active trace gases, i.e., carbon dioxide (CO_2) and methane (CH_4). Although a variety of methods is used in such studies, most flux measurements are made either at the plot scale (10^{-2}–10^{0} m^2), using various forms of chamber, or at the patch scale (10^{4}–10^{5} m^2), using the eddy covariance (EC) technique. In order to use such flux measurements to provide estimates of components of the natural carbon cycle at landscape (10^{1}–10^{2} km^2), regional (10^{3}–10^{6} km^2), or hemispheric to global land surface (10^{7}–10^{8} km^2) scales, they must be "upscaled" using some form of model. If such models do not explicitly take into account heterogeneity in the cover of vegetation on the land surface, it is likely that their results will be inaccurate [*Oechel et al.*, 1998] because land surface–atmosphere fluxes of CO_2 differ between vegetation types. Upscaling models therefore frequently use some form of vegetation or land cover map, often derived from Earth observation (EO) data, to assess the areal extent of each surface type. The overall flux for the more extensive area is then estimated by calculating the area-weighted sum of fluxes measured for the various land surface types [e.g., *Heikkinen et al.*, 2004; *Soegaard et al.*, 2000]. Other studies have used continuous variables recovered from EO data, such as the normalized difference vegetation index, as the basis for weighting measured fluxes to derive estimates for more extensive areas [e.g., *Kim et al.*, 2006; *Vourlitis et al.*, 2000].

[3] An important assumption implicit in such upscaling is that the plot- or patch-scale measurements are not biased in

[1]Institute of Ecosystem Science, School of Biological and Biomedical Sciences, University of Durham, Durham, UK.
[2]Department of Applied Mathematics, University of Sheffield, Sheffield, UK.
[3]Centre for Ecology and Hydrology, Wallingford, UK.
[4]Institute of Atmospheric and Environmental Sciences, School of Geosciences, University of Edinburgh, Edinburgh, UK.

0886-6236/08/2007GB003027

any way as a result of the measurement techniques employed. Given that plot- and patch-scale measurements are both used in some cases, a further assumption is that the flux estimates they provide are equivalent. Although a number of previous studies have compared plot- and patch-scale measurements of CO_2 flux, the majority have chosen homogeneous patches [e.g., *Dore et al.*, 2003; *Griffis et al.*, 2004], even when the study has included aircraft measurements at landscape scales [*Smith et al.*, 2003]. In some studies unvegetated areas have been selected [*Kabwe et al.*, 2005], or the position of the EC instrument tower has been adjusted during the field campaign in order to maximize homogeneity of the patch within the measurement footprint at any time [*Reth et al.*, 2005]. *Heikkinen et al.* [2002], however, measured fluxes for a patterned boreal mire at Kaamanen, Finland, with three distinct surface types. Despite the predominance of one surface type, which accounted for 60% of the surface area, and the minority occurrence of the third (10%), they found a difference between the CO_2 flux measured by EC and an estimate obtained by areally weighting chamber measurements. In contrast, a study of an oceanic mire at Glencar, Ireland, with a patterned surface comprising four surface types found close correspondence between estimates of net ecosystem exchange (NEE) made from EC data and from chamber measurements using an areal weighting that took into account wind direction [*Laine et al.*, 2006]. The spatial scale of heterogeneity of this oceanic mire surface, however, was relatively small ($\sim$1 m^2), and its surface pattern was homogeneous. Furthermore, NEE varied by only 30% between its surface types, all of which were predominantly carbon sinks. The surface type accounting for 30% of the mire surface at Kaamanen, in contrast, was generally a net source even during daylight in the middle of the growing season, whereas the other two surface types were net sinks during daytime.

[4] Potential future temperature increases are projected to be greatest at high latitudes where tundra predominates [*Cubasch et al.*, 2001]. Because tundra soils are highly organic and represent an important reservoir of carbon, much of which is susceptible to relatively rapid microbial decomposition [*Sjogersten et al.*, 2003; *Sjogersten and Wookey*, 2002], such warming has the potential to generate a positive feedback as the NEE of tundra areas is likely to become more positive (that is, the balance between photosynthetic uptake and respiratory release is shifted toward the latter). We follow the micrometeorological convention; thus a positive NEE represents a net flux of CO_2 from the land surface to the atmosphere and vice versa. CO_2 fluxes of Arctic tundra regions are thus likely to be an important component of the global carbon cycle, and estimation of their overall contribution to the global land surface–atmosphere net CO_2 flux is an important scientific goal [*McGuire et al.*, 2002]. Although tundra areas often exhibit marked heterogeneity, usually related principally either to interactions between topography, vegetation, and snow cover (Figure 1a) or to fossil or active permafrost features, previous studies of CO_2 fluxes at tundra localities generally have examined relatively homogeneous patches [e.g., *Corradi et al.*, 2005]. In the present study a combination of EC and plot-scale chamber measurements of CO_2 flux was used to investigate the sensitivity of NEE of a patch of heterogeneous tundra to irradiance and temperature; six land surface types form the vegetation mosaic of this tundra patch. We also quantified the differences between overall NEE estimates made from EC data and those made by areally weighting chamber measurements. The relationships between NEE, irradiance, and temperature for the chamber and EC measurements were modeled using an approach that provides estimates of the uncertainties in the relationship [*Williams et al.*, 2006]. A footprint model (flux source area model (FSAM)) [*Schmid*, 1994, 1997] was then used to model the varying contributions to the flux measured at the EC tower made by the six elements of the vegetation mosaic being sampled as meteorological conditions varied and to estimate the uncertainties in these flux contributions during each half-hour observation interval. Finally, the results from these two models were used to model the flux measured at the EC tower according to the prevailing meteorological conditions, and the results were compared to the flux estimated directly from the EC measurements and to fluxes modeled using various alternative approaches. The results indicate a substantial bias between the two measurement approaches that results in a substantial discrepancy between the flux estimated from EC data and that obtained by upscaling from chamber measurements, despite the upscaling model taking into account the varying meteorological conditions. This bias exceeds in magnitude the uncertainties in the upscaled modeled fluxes.

2. Study Site

[5] The study site is an area of heterogeneous tundra just beyond the tree line near Abisko in northern Swedish Lapland (68°18′N, 18°51′E, 730 m above sea level). The EC instrument tower was located on a broad terrace on the northern flank of the hill Nissonsnuohkki, the long axis of the terrace being aligned more or less with the prevailing southwesterly wind direction. Six mosaic elements were discriminated in the tundra at the site, each representing a visually distinctive vegetation class that accounted for a substantial fraction of the land cover (Figure 1a). The six elements are described as follows.

[6] 1. The fell field (FF) consists of very sparsely vegetated areas dominated by bare rock and gravel. Higher plants, including prostrate dwarf shrubs, mainly *Betula nana* and *Empetrum nigrum* ssp. *hermaphroditum*, typically cover no more than $\sim$10% of the ground, although bryophytes, principally *Polytrichum* spp. and especially lichens, notably *Alectoria ochroleuca*, *Cetraria* spp., and *Cornicularia* spp., may cover up to $\sim$30%.

[7] 2. Open *Empetrum* heath (OE) consists of dry heath vegetation that covers usually $\sim$50% of the ground, dominated by low-growing (typically $\sim$5 cm) *Empetrum nigrum* ssp. *hermaphroditum*. A continuous carpet of bryophytes generally is present beneath the *Empetrum*. Bare rock and gravel dominate the remaining $\sim$50%, although usually with a similar extent of bryophyte and lichen cover present to that in the fell field areas.

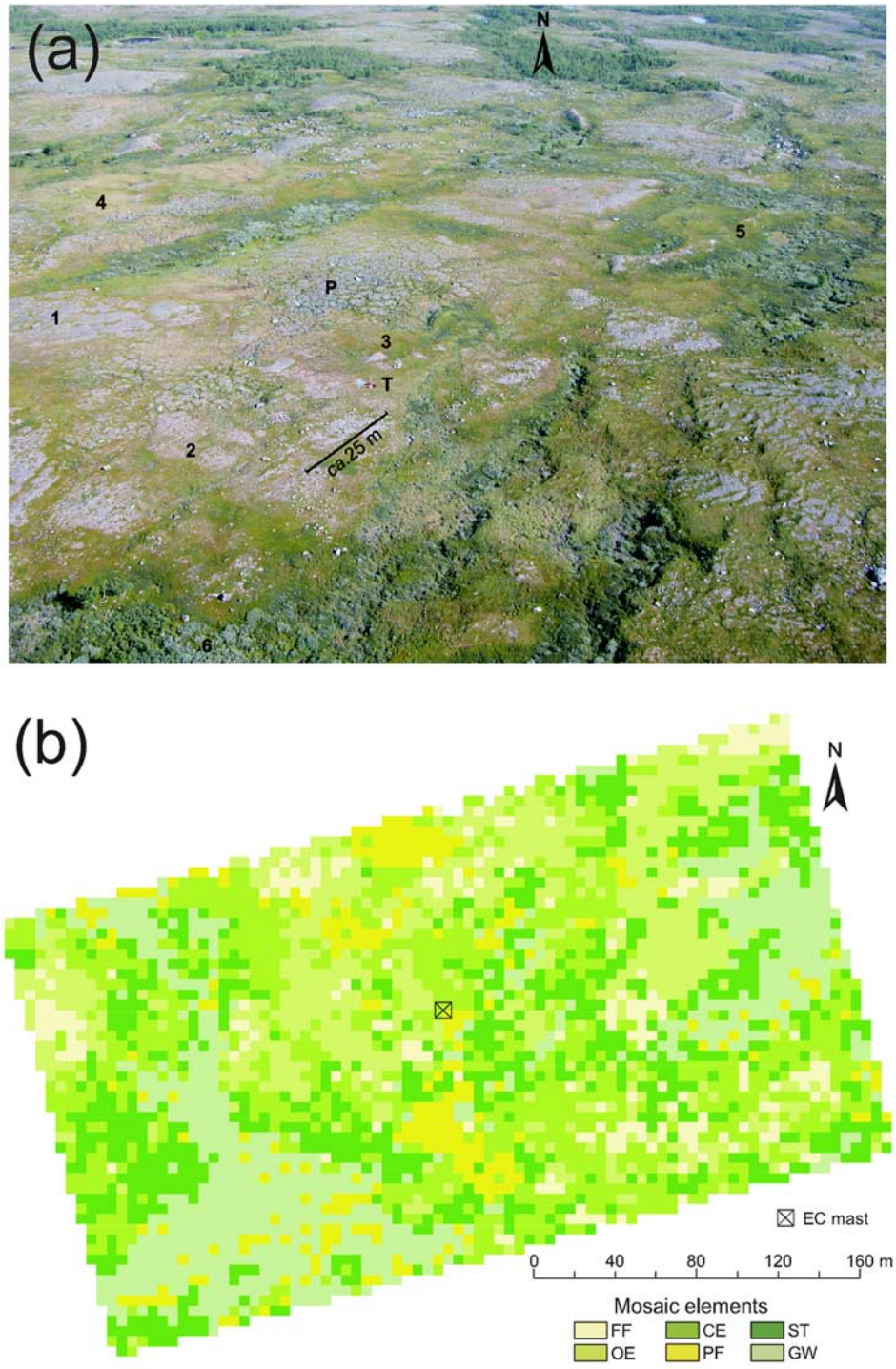

Figure 1. (a) Aerial view across the study site. Study site viewed obliquely from above and to the south. The position of the eddy covariance instrument tower (T) is indicated, as is the approximate scale in that part of the view where it is located. Examples of each of the six principal elements of the land cover mosaic are indicated as follows: 1, fell field; 2, open *Empetrum* heath; 3, closed *Empetrum* heath; 4, poor fen; 5, shrub tundra; and 6, gray willow scrub. A prominent area of fossil-patterned ground (P) characterized by finer-scale heterogeneity than the landscape generally also is indicated. (b) Land cover–type mosaic in the patch sampled by eddy covariance measurements. Six mosaic elements were recognized (see descriptions in text) and mapped on a 5 m grid across the patch sampled by the eddy covariance measurements. The six elements are FF, fell field; OE, open *Empetrum* heath; CE, closed *Empetrum* heath; PF, poor fen; ST, shrub tundra; and GW, gray willow scrub.

[8] 3. Closed *Empetrum* heath (CE) consists of dry heath vegetation in which the vegetation cover is usually almost 100%, dominated by low-growing (typically ~5–10 cm) *Empetrum*. A few other dwarf shrub species also are typically present, as is a more or less continuous carpet of bryophytes beneath the *Empetrum*.

[9] 4. Poor fen (PF) areas are characterized by saturated organic soils dominated by a variety of relatively short (typically ~10–25 cm) *Carex* spp. and other Cyperaceae. Bryophytes are present throughout the dense sward that covers ~80–100% of the ground. Although conveniently considered as a single class in terms of their physiognomy, these areas exhibit a high level of floristic diversity, much of which is probably related to water quality.

[10] 5. In the shrub tundra (ST) community, *Betula nana* forms the upper layer, with *Empetrum* and *Vaccinium* spp. growing beneath the *Betula* canopy and in turn a generally continuous bryophyte carpet beneath these. Vegetation cover is close to 100%, and the *Betula* is generally ~10–30 cm tall.

[11] 6. Gray willow scrub (GW) areas are dominated by *Salix glauca*, covering ~60–100% of the ground and growing to ~50–150 cm in height. Other *Salix* spp., notably *S. lanata*, are present more sparsely, and a variety of dwarf shrubs also are often present, including *B. nana* and *Vaccinium* spp. growing beneath and among the *S. glauca*. A diverse range of forbs and graminoids typically is present in the understory.

[12] The distribution of these six mosaic elements in the patch sampled by the EC measurements was mapped at a 5 m resolution (Figure 1b). Real-time kinetic GPS (5700 base station plus 5800 rover, Trimble Navigation Ltd., Sunnyvale, California, USA) was used to locate the intersections of a 5 m grid (220 m × 400 m) extending across the patch and aligned along the terrace on which the EC instrument tower was sited (Figures 1a and 1b). At each grid intersection the predominant mosaic element was recorded, the elements being readily distinguishable by simple visual inspection. With the exception of fell field, the elements occupied relatively even proportions of the grid, no element being markedly more extensive than the remainder: FF, 0.075; OE, 0.169; CE, 0.210; PF, 0.154; ST, 0.210; and GW, 0.183.

3. Carbon Dioxide Flux Measurements

3.1. Plot-Scale Measurements

[13] NEE was determined within two 1 × 1 m plots on each of the FF, CE, PF, and GW mosaic elements and three 1 × 1 m plots on the ST mosaic element. Measurements were not made on the OE element type. Measurements were made between 22 and 24 July (days of year (DOY) 204–206) and between 10 and 12 August 2004 (DOY 223–225), during the second half and near the end of the polar day at this latitude. CO_2 fluxes were measured using a LI-COR 6400 portable photosynthesis system (LI-COR Inc., Lincoln, Nebraska, USA) connected to a 1 × 1 × 0.25 m Plexiglas chamber [*Shaver et al.*, 2007; *Street et al.*, 2007; *Williams et al.*, 2006].

[14] Two or three net CO_2 flux measurements were made at full sunlight, followed by one or two measurements made at successive levels of shading (usually three). Finally, a measurement was taken in complete darkness (dark respiration). All measurements lasted on average ~2 min each. Data were subsequently analyzed as detailed by *Street et al.* [2007], and light response curves were constructed. Error in the observations must be specified in the modeling component of this study (see section 4); in the case of the chamber measurements this was estimated as the variance in NEE observations made over the same mosaic element and within 100 μmol m^{-2} s^{-1} photosynthetically active radiation (PAR), considering the July and August measurements separately [*Williams et al.*, 2006]. For some mosaic elements these variances were large because the replicate sites, although being of the same vegetation type in terms of our classification, varied markedly in their leaf area and vegetation height. However, as each mosaic element was being modeled as a "generic" type, this approach appropriately represented the variation found within the elements recognized by our classification scheme.

3.2. Patch-Scale Measurements

[15] Measurements of the turbulent fluxes of sensible and latent heat, CO_2, and momentum were made by the eddy covariance technique using a combination of a three-dimensional sonic anemometer (Solent R2, Gill Instruments Ltd., Lymington, UK) and an open path infrared gas analyzer (LI-7500, LI-COR Inc.). The instruments were located on a mast at a height of 3 m, well above the surface roughness sublayer but within the well-mixed surface boundary layer above the short (generally <0.2 m) vegetation. Raw 21 Hz outputs from the two instruments were recorded by a rugged laptop computer (Husky FC-486, Husky Technology Ltd., Coventry, UK) in 30-min blocks on 512 Mb compact flash memory cards. Edisol [*Moncrieff et al.*, 1997] data acquisition software was used; this also provided uncorrected half-hourly means of the fluxes. Raw data were postprocessed using EdiRe; flux conversions and calibrations, as well as corrections for flux losses due to density variations, sensor separation, path lengths, and response times, were applied (software package developed by J. B. Moncrieff, School of Geosciences, University of Edinburgh, available at http://www.geos.ed.ac.uk/abs/research/micromet/EdiRe/). The postprocessed data provide half-hourly means of the turbulent vector and scalar measurements, as well as of the fluxes. An automatic meteorological station was located adjacent to the mast with the EC instruments. At a height of 2 m this recorded incoming and reflected short-wave radiation, incoming all-wave radiation, incoming and reflected photosynthetically active radiation, air temperature, precipitation, and wind speed and direction. This study focuses on a 40-day period at the peak of the growing season in 2004, from 13 July (DOY 195) until 21 August (DOY 234), encompassing 1920 half-hour observation periods. EC NEE measurements were quality controlled by excluding any half hour during which precipitation was recorded (221 observations), because rainfall interferes with the functioning of an open path infrared gas analyzer, or when NEE was negative (indicating photosynthetic uptake) but incoming PAR was recorded as less than 10 μmol m^{-2} s^{-1} (a further 31 observations). In order to produce a continuous time

series for NEE, those 252 observations that were excluded were gap filled using the mean NEE value for the missing time of day half hour. Half-hourly means were calculated separately for two 20-day periods, DOY 195–214 (period 1, late July) and DOY 215–234 (period 2, early August), and the half-hour mean for the appropriate period was used to gap fill (Figure 2a). For each NEE measurement, "error" was estimated from the error variance (σ^2) found when binning observations that were made under similar environmental conditions. Conditions were considered to be "similar" to those for an NEE measurement for which uncertainty was estimated (the "target" measurement) when they were (1) within 5 days of the target measurement, in order to account for phenological variation; (2) at a PAR value within 100 μmol m^{-2} s^{-1} of that of the target measurement; and (3) at a temperature within 5°C of that of the target measurement. Binning was performed separately for measurements made during the two 20-day periods defined earlier.

4. Modeling Carbon Dioxide Fluxes

4.1. Photosynthetic Irradiance Response and Temperature-Sensitive Respiration (PIRT) Model

[16] The chamber and EC measurements of NEE were used to constrain PIRT models [*Williams et al.*, 2006] for each of the five mosaic elements on which chamber measurements were made and for the EC data. The model has the form

$$\mathrm{NEE} = R_b e^{\beta T} - \frac{P_{\max} I}{k + 1}, \quad (1)$$

where $P_{\max}$ is the rate of light-saturated photosynthesis (μmol CO_2 m^{-2} s^{-1}), k is the half-saturation constant of photosynthesis (μmol PAR m^{-2} s^{-1}), I is the incident photosynthetic photon flux density (μmol m^{-2} s^{-1}), R_b is basal ecosystem respiration (μmol CO_2 m^{-2} s^{-1} at 0°C), and β (°C^{-1}) quantifies the relative increase in respiration with air temperature T (°C). All four parameters in the model ($P_{\max}$, k, R_b, and β) were found using the maximum likelihood technique [*van Wijk and Bouten*, 2002]. Maximum likelihood technique estimators aim to find the parameter values that make the observed data most likely. They are able to represent measurement error and thus provide a basis for both evaluating the adequacy of model fit and providing a multivariate parameter confidence region within which the true parameter values fall with a given confidence level. Optimal parameters are found by minimizing the objective function:

$$O(p) = \sum_{i=1}^{n} \frac{1}{\sigma_{yi}^2} \left[y_{i,\mathrm{meas}}(x_i) - y_{i,\mathrm{mod}}(x_i : p) \right]^2, \quad (2)$$

where n is the total number of measurements, p is the number of model parameters, $y_{i,\mathrm{meas}}(x_i)$ is the measured value of output variable y at the value x_i of the driving variable x, $y_{i,\mathrm{mod}}(x_i; p)$ is the modeled value of the output variable at the value x_i of the driving variable x given the parameters p, and σ_{yi}^2 is the measurement error variance for each of the observations. The minimum sum of squares follows a chi-square (χ^2) distribution with $n - p$ degrees of freedom. A Monte Carlo–style approach was used to determine the value of the objective function for combinations of all four parameters, generating parameter confidence regions. Forty values for each parameter were chosen, equally spread between specified maximum and minimum values ($1 < P_{\max} < 30$, $100 < k < 1000$, $0.1 < R_b < 3$, and $0.01 < \beta < 0.2$) which were selected on the basis of work by *Williams et al.* [2006]. A χ^2 test was used to determine which of the 2.56×10^6 parameter sets produced model results within a 95% confidence interval of the observations.

[17] In nearly all cases the number of acceptable parameter sets that fitted these uncertain observations was high, typically $1.0–5.0 \times 10^4$ of the 2.56×10^6 combinations examined. NEE was then modeled for periods 1 and 2 for each of the five mosaic elements measured, and for the EC data, for 0–2000 μmol m^{-2} s^{-1} PAR at 100 μmol m^{-2} s^{-1} PAR intervals, and for 0–20°C at 1°C intervals (400 input points in total), randomly sampling the relevant acceptable parameter set 500,000 times for each point. Mean and σ^2 of NEE for each combination of temperature and irradiance were calculated from the modeled values. Uncertainty in the model predictions increased in each case at higher temperature and irradiance. This reflects the range of values used in the initial parameter fitting. That is, few of the measurements were made either at high light levels or high temperatures; thus observational uncertainty, and hence also modeled uncertainty, is higher under such conditions. The mosaic elements differ principally with respect to the absolute magnitude of the measured and modeled NEE. Elements characterized by taller-growing shrub (GW) or dwarf shrub (ST) vegetation achieve higher negative NEE values, i.e., greater photosynthetic uptake, probably because these communities have a higher leaf area index than do the shorter-growing *Empetrum* (CE), poor fen (PF), and fell field (FF) elements [*Street et al.*, 2007].

[18] The PIRT model was then used to estimate mean and σ^2 of NEE for each mosaic element for each half-hour observation interval during the two 20-day study periods (Figure 2b); 500,000 model realizations were made for each mosaic element and half-hour interval, randomly sampling the relevant acceptable parameter set for each mosaic element and period. Half-hour mean PAR observed at the meteorological station was used to drive the model for all elements, along with half-hour mean within-canopy air temperature measurements made for FF, EC, PF, and GW. The latter temperature measurements were made at 10 s intervals at a number of positions within each canopy type using fine bead thermocouples (Type-T TTSS-18E-12, Omega Engineering Ltd., Manchester, UK); measurements were logged and half-hourly means were stored using a Campbell CR 10X data logger (Campbell Scientific Inc., Logan, Utah, USA). The values used to drive the model were the means of the half-hourly means for those sensors within each canopy type. GW within-canopy air temperature measurements were also used for ST because no direct observations were available for this mosaic element. The parameter sets derived from chamber measurements made in July were used for period 1, whereas those derived from the August chamber measurements were used for period 2.

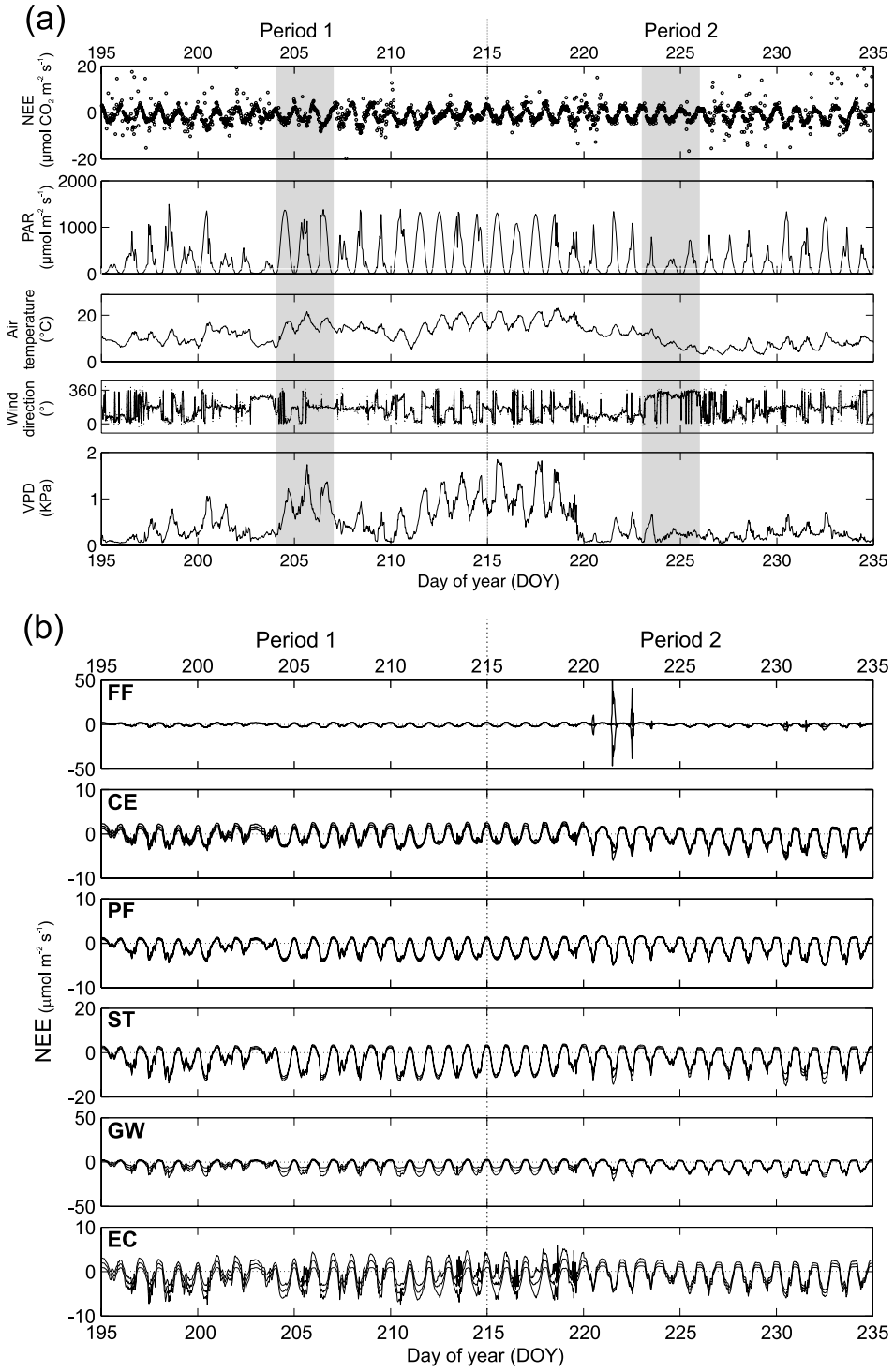

Figure 2. (a) NEE and driving variables measured during the study period. NEE calculated from EC data for CO_2 flux. PAR, air temperature, wind direction, and vapor pressure deficit from an adjacent meteorological station. The 40-day study period extended between 13 July and 21 August 2004. The shaded areas highlight periods when chamber measurements were made. (b) NEE simulated for the study period. NEE (mean ± 1 σ^2) were simulated using PIRT models for five mosaic elements and for the EC data; parameter sets were constrained by relevant measurements made during the corresponding 20-day period. All models were driven using mean PAR observed at the meteorological station and an appropriate measure of mean temperature for each half-hour interval. For the mosaic element models, temperature was the mean within-canopy air temperature for that element; for the EC model, temperature was the mean of the five mosaic element within-canopy air temperatures.

The acceptable parameter sets fitted to the EC data for the two periods similarly were used to model NEE, as estimated from EC, for each half-hour interval of the 40-day study period (Figure 2b). In this case the model was driven using half-hour mean PAR observed at the meteorological station and the mean of the four half-hour mean within-canopy air temperatures for the mosaic elements in which measurements were made. In all cases the variance in NEE is highest on the warmest days because the PIRT model is least well constrained at these high temperatures. Individual days during period 2 with high variance for the individual mosaic elements, most noticeable for FF, reflect this limitation of the model. Overall, variance in modeled NEE is greatest for EC; this is a result of the larger number of parameter sets that give an acceptable fit to the much larger data set of EC measurements. Although, as discussed above, the magnitude of the modeled NEE differs between mosaic elements, all five show a clear diurnal pattern with negative daytime NEE values and positive nighttime values; furthermore, even the very open and sparsely vegetated FF has a net negative NEE over both 20-day periods.

4.2. Footprint Model

[19] The footprint model used in this study is the flux source area model [*Schmid*, 1994, 1997]. This is an analytical model, based on work by *Horst and Weil* [1992, 1994], providing an approximate solution to the advection-diffusion equation proposed by *Vanulden* [1978] and *Gryning et al.* [1987] to determine the ''field of view'' of the EC flux sensors. This model calculates a source weight function (footprint function) indicating the relative contribution of ground level point sources within the source area to the signal recorded by the sensors mounted at a height z_m using the Obukhov length (L), friction velocity (u^*), standard deviation of crosswind speed fluctuations (σ_v), roughness length (z_0), and wind direction. The source weight function is an asymmetric bell-shaped curve extending upwind from the EC mast, rising to a maximum at some distance upwind from the sensors and falling off smoothly on all sides. The integral beneath the function expresses the total surface influence on the signal measured at the sensor; the function can be thought of as analogous to a probability density function giving the probability of a source at some point within the source area influencing the sensor [*Schmid and Lloyd*, 1999]. The critical assumption made when using this source area function over a nonuniform surface, such as the heterogeneous tundra of our study site, is that it is primarily energy, water, and carbon fluxes that are affected by spatial variation in the surface character, whereas the momentum flux is affected to a much lesser extent, and the mechanical setting of the exchange processes is thus approximately uniform throughout the entire potential source area for the instrument. Both this assumption and the model assumption that all fluxes originate at the zero-plane displacement height (z_d) seem reasonable in the present study, given that the vegetation of each mosaic element is uniformly relatively short and the topography of the site is reasonably smooth. The model was applied only during periods of neutral and moderately unstable atmospheric stability ($-0.1 < z_m/L < 0.1$) and with a limited range of crosswind turbulence intensity ($1 < \sigma_v/u^* < 6$). Here z_d was estimated as 0.1 m on the basis of measured vegetation height and z_0 was assumed to be uniform across the potential source area and to have a value of 0.005 m. FSAM was driven by EC data for the 40-day study period filtered to include only half-hour observation intervals during which conditions satisfied the suitability criteria discussed above (573 from the total of 1920). The source area from which 90% of the fluxes were derived was determined for each observation interval, and source weights within this area were calculated for a 5 m $\times$ 5 m grid. This grid of source weights was then aligned upwind from the EC mast and superimposed upon the vegetation map. The source weights overlying each of the six mosaic elements were then summed to give a ''source fraction'' for each mosaic element.

[20] Observational errors in the vegetation mapping and in the EC and wind direction measurements, as well as errors in the FSAM model and its underlying statistical assumptions, potentially all contribute to uncertainty in the calculated source fractions that may be substantial. This was addressed first by determining the sensitivity of FSAM to the driving variables using Gaussian Emulation Machine for Sensitivity Analysis (GEM-SA) software [*Kennedy et al.*, 2006; *Kennedy and O'Hagan*, 2000, 2001] (see also http://ctcd.group.shef.ac.uk/gem.html). A Latin hypersquare sampling routine was used to select 400 parameter sets from uniform distributions of the possible ranges described above for z_m/L, σ_v/u^*, and wind direction. The sensitivity analysis clearly demonstrated that for each of the six mosaic elements wind direction alone accounted for 75–85% of the variation in source fraction. This indicated that although the footprint model and EC-derived variables have unknown uncertainties, wind direction accounts for most of the variation in the FSAM model output. The standard deviation (σ) of wind direction had, however, been recorded for each half-hour observation interval. The FSAM model code therefore was modified to calculate the source fractions 500 times for each half-hour observation interval, varying the wind direction around the recorded mean wind direction according to the recorded σ and random numbers drawn from a normal distribution. The mean and σ^2 of the source fraction for each mosaic element for each of the 573 half-hour observation intervals that met the suitability requirements were then calculated. Source fractions for the remaining 1347 observation intervals to which FSAM could not be applied were gap filled using their mean wind direction. Source fractions calculated for the intervals of favorable conditions were binned into eight 45° wind direction sectors, and the mean and σ of the source fractions were calculated for each bin. These values were then used to gap fill, enabling a continuous time series of mean source fractions and their σ^2 to be constructed for the entire 40-day study period. The time series of source fraction for each of the six mosaic elements is illustrated in Figure 3. As might be expected, given that it accounts for the smallest fraction (0.07) of the mapped area, the source fraction for FF never exceeds 0.1. CE and ST, however, both of which account for the same fraction of the mapped area (0.21), differ markedly with respect to their maximum source fraction, ST at times reaching a source fraction exceeding 0.5, whereas CE only

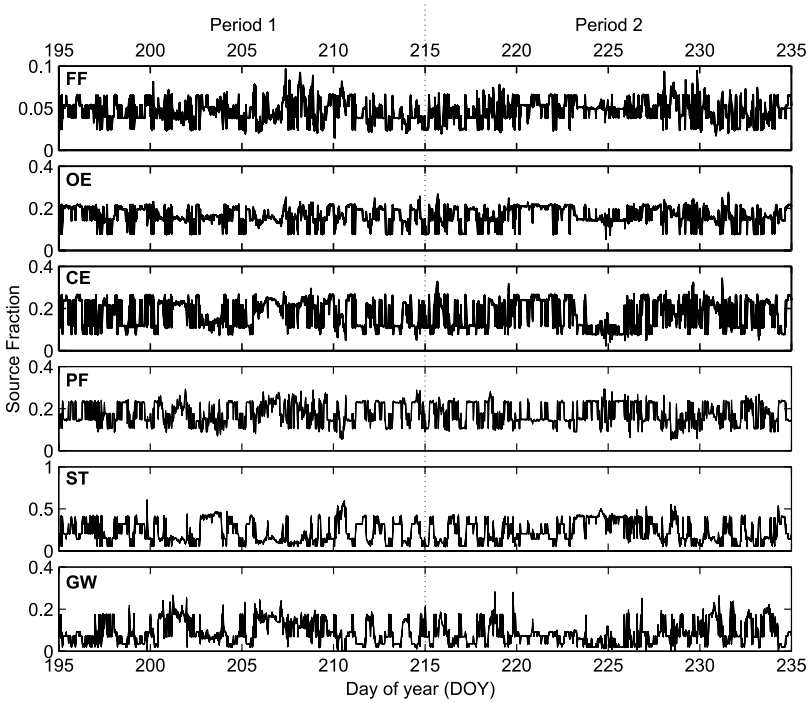

Figure 3. Source fractions simulated for the study period. Mean source fraction for each mosaic element for half-hour observation intervals during the study period (σ^2 of source fractions are of too small a magnitude to be illustrated) simulated using the FSAM model. Source fraction is the contribution of that mosaic element to the source area (footprint) from which 90% of the fluxes measured by the EC instruments are derived during the half-hour observation interval.

rarely exceeds 0.3. The source fraction for GW, in contrast, only rarely exceeds its fraction of the mapped area (0.18) and for much of the time is less then half this value.

5. Scaling From Plot to Patch

[21] Three approaches were used to upscale the modeled NEE for the mosaic elements to the footprint of the EC mast in order to allow comparison both to the NEE calculated directly from the EC observations and to the NEE modeled from the EC data. A representative 10-day period is shown in Figure 4. "Footprint" NEE was simulated using the FSAM footprint model coupled to the PIRT model. For each half-hour interval 500,000 realizations of the combined model were computed, randomly sampling the acceptable parameter sets for each mosaic element and also the 500 FSAM-derived source fractions for that interval. The σ^2 of the simulated NEE in this case thus reflects uncertainty in both models. "Mapped" NEE uses the mapped proportions of each mosaic element (FF, 0.07; OE, 0.17; CE, 0.21; PF, 0.15; ST, 0.21; and GW, 0.18) as fixed source fractions, whereas "Equal" NEE uses equal proportions of each mosaic element (i.e., 0.17) as fixed source fractions. For both mapped and equal NEE simulations, fluxes were simulated for each half-hour interval for each mosaic element using the PIRT model; 500,000 realizations of the model were computed, randomly sampling the acceptable parameter sets for each mosaic element. The σ^2 of the simulated NEE in these latter two cases thus reflects uncertainty in the PIRT model alone. "EC model" NEE is equivalent to the bottom plot of Figure 2b.

[22] Figure 5a shows a 1:1 plot of footprint NEE against EC observations. The slope of the line is 0.6 (significantly less than 1), with an intercept of -0.9, indicating an underestimation of nighttime respiration by the model. However, the scatter of points also appears to represent an overestimation of photosynthesis (i.e., more negative NEE). Figure 5 also shows the residuals between footprint NEE and EC observations plotted against PAR (Figure 5b) and vapor pressure deficit (VPD) (Figure 5c). Scatter of the residuals indicates a negative bias for values of PAR above $\sim$800 μmol m^{-2} s^{-1}, indicating an overestimation of CO_2 uptake at high irradiance (Figure 5b) and at very low (i.e., nighttime) values of PAR (<25 μmol m^{-2} s^{-1}), a consequence of underestimation of nighttime respiration by the model. Figure 5c also suggests a negative bias in the residuals at VPD values greater than $\sim$1.2 kPa. Very similar patterns were found in the residuals for the other upscaling approaches: mapped NEE and equal NEE (data not shown).

[23] Cumulative NEE for the 40-day study period was calculated from the modeled NEE values for the half-hour observation intervals for the six individual mosaic elements and for the EC data. For the purposes of upscaling, OE (not measured at plot scale) is taken to be a 50:50 mix of FF and CE mosaic elements. Mean and σ^2 of the modeled NEE were calculated from the NEE values for each of the 500,000 model realizations for each half-hour interval. Cumulative NEE was also calculated from the NEE values

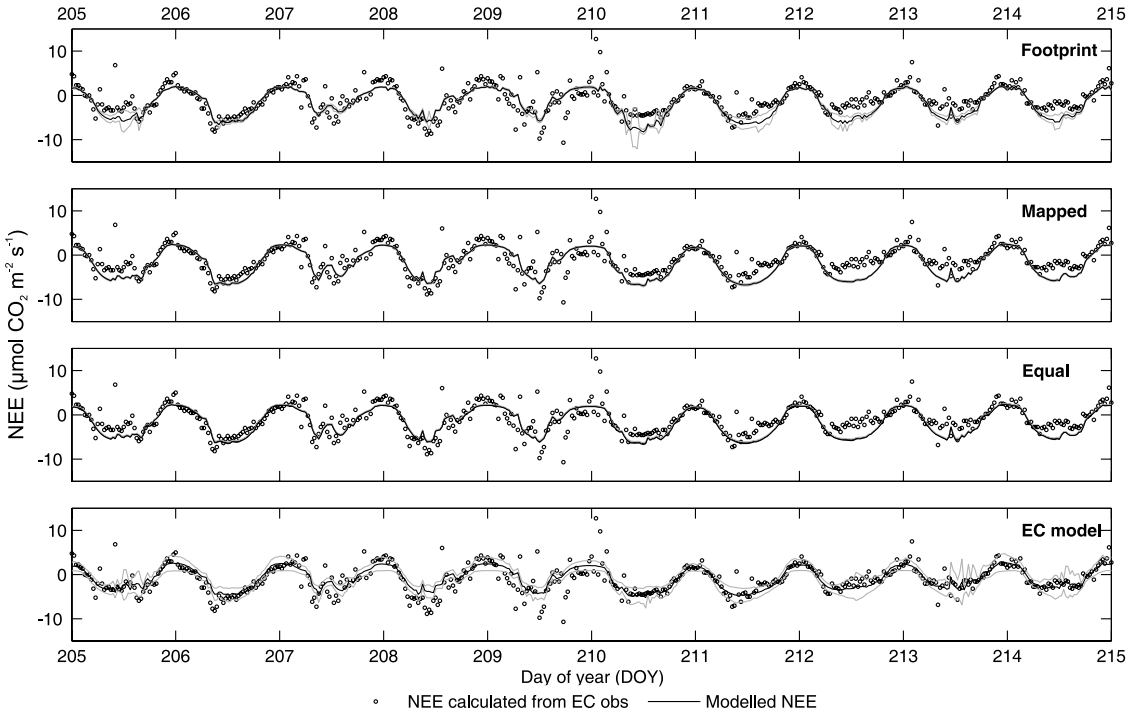

Figure 4. Simulated and observed NEE time series for the study period. NEE time series (mean ± 1 σ^2) for a representative 10-day period within the study period, simulated using three upscaling approaches. "Footprint" indicates that simulated mosaic element NEEs were upscaled using simulated source fractions. "Mapped" indicates that upscaling used the (fixed) fractions of each mosaic element found in the 220 m × 400 m area surveyed. "Equal" indicates that upscaling used equal contributions from each mosaic element. The NEE time series simulated by the PIRT model for the EC data ("EC model") is included for comparison. In all cases the simulated time series is overlaid onto the NEE calculated from the EC measurements for the half-hour observation intervals.

calculated from the gap-filled time series of EC observations for the 40-day study period. Cumulative NEE for the 40 days ranged from -38.2 ± 66.7 g CO_2 m^{-2} for the FF mosaic element to -581.1 ± 240.5 g CO_2 m^{-2} for GW; mean values were all negative, indicating net uptake of CO_2 over the study period by all mosaic elements (Table 1). A similar approach was used to calculate cumulative NEE from the upscaled fluxes simulated by the three upscaling approaches (Figure 6 and Table 1). The results showed that cumulative NEE simulated by the footprint upscaling approach did not differ significantly from that simulated either by the mapped or equal upscaling approaches. All three approaches, however, gave cumulative negative NEE estimates >60% greater in absolute value than the cumulative NEE value calculated from the EC observations. In contrast, the cumulative NEE simulated by the EC model was ~23% less in absolute value than that calculated from the EC observations, although the very high uncertainty of the values simulated by this model results in all of the other estimates of cumulative NEE, with the exception of those for the ST and GW mosaic elements, falling within ±1 σ^2 of the mean simulated value.

6. Discussion

[24] The results presented here raise two interesting questions: First, why do the three alternative upscaling approaches give results that do not differ significantly (Figures 4 and 6) despite the large variations in source fraction between half-hour observation intervals (Figure 3) and variation in meteorological conditions, especially wind direction, and hence in the flux footprint? Second, what is the cause of the large bias between NEE values estimated by upscaling from chamber measurements and those calculated from EC data?

[25] As Figures 1a and 1b illustrate, the heterogeneity in the land surface of our study site does not have a uniform spatial scale across the site, some patches being only a single 5 m × 5 m grid cell and others extending to >100 m in at least one dimension. This nonuniform heterogeneity, as well as its length scale typically of 10^1–10^2 m, contrasts markedly with the rather uniform and fine-scale (~1–3 m) heterogeneity reported by *Laine et al.* [2006] for the patterned mire site that they studied. Substantial and significant differences are seen between NEE values simulated by PIRT models fitted for the five mosaic elements in which chamber measurements were made (Figure 2b), resulting in significant differences in cumulative NEE across the study period (Table 1). In particular, the ST and GW mosaic elements give a significantly more negative cumulative NEE than either that simulated by the PIRT model fitted to the EC data or that calculated from the EC observations, whereas the FF and CE mosaic elements give a significantly

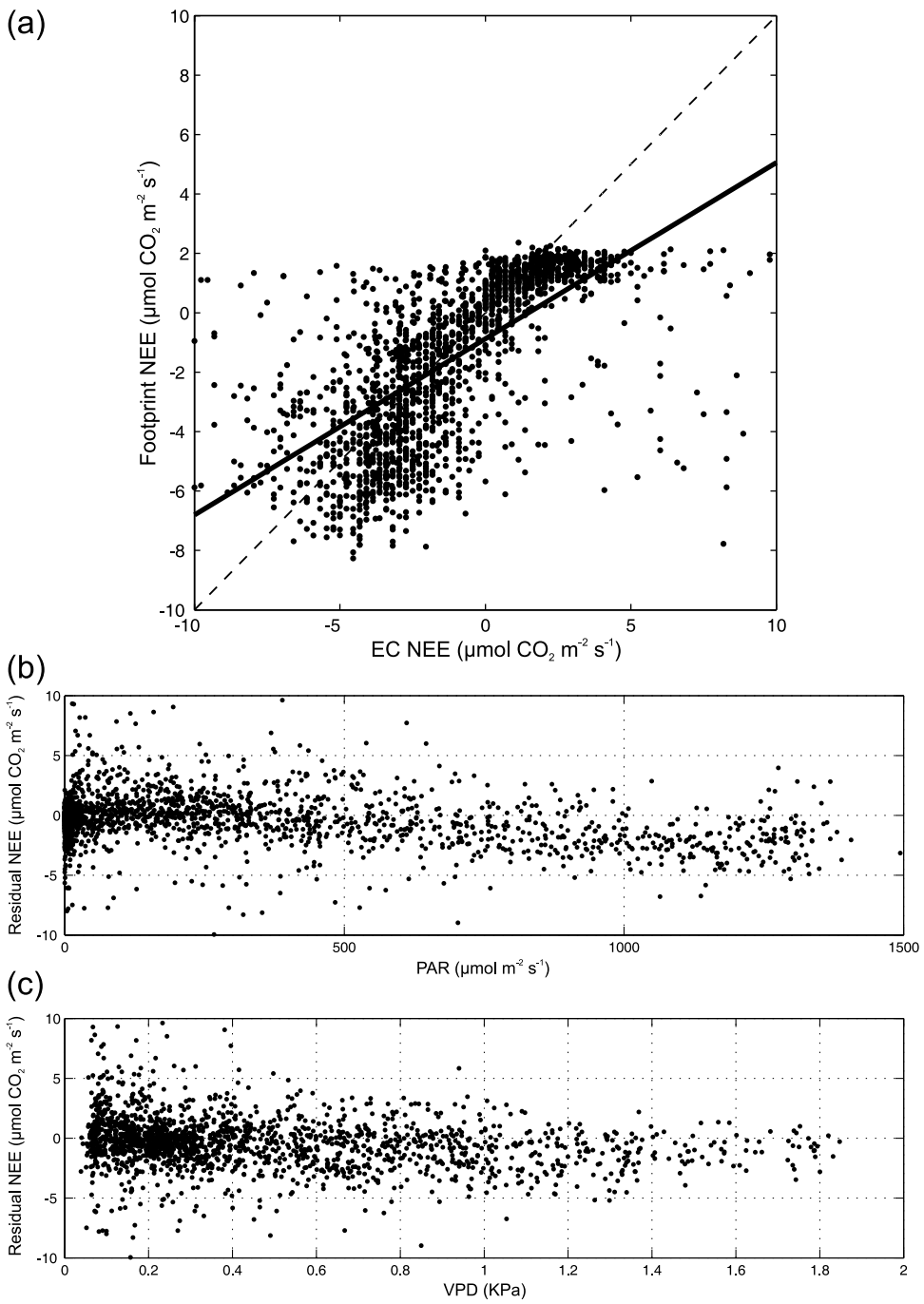

Figure 5. (a) Simulated footprint NEE versus observed NEE. Plots of NEE simulated using footprint upscaling approach (see text and Figure 4 for details) versus observations. Plotted points represent mean NEE values for half-hour observation intervals plotted against simulated NEE for those intervals. The solid line indicates the regression line, and the dashed line indicates the 1:1 line. Residuals between simulated footprint and observed NEE (b) versus PAR and (c) versus VPD. Plots of the residuals calculated between observed NEE and NEE simulated using the footprint upscaling approach for half-hour observation intervals versus mean PAR and VPD measured at the meteorological station adjacent to the eddy covariance mast for those observation intervals.

less negative cumulative NEE than that calculated from the EC observations. Therefore, if the upscaling using the footprint model estimated source fractions in proportions different from the mapped proportions or from equal areas, then footprint NEE would be significantly different from the two alternative upscaling approaches. Table 2 contains the fractions of vegetation types used in the mapped and equal upscaling and the cumulative source area fractions calcu-

Table 1. Cumulative NEE Over 40-day Study Period

	Cumulative NEE Mean ± 1 σ^2 (g CO_2 m^{-2})
Mosaic element	
FF	−38.2 ± 66.7
OE	−53.5 ± 30.4
CE	−68.7 ± 54.7
PF	−133.3 ± 21.5
ST	−427.8 ± 97.6
GW	−581.1 ± 240.5
Upscaling approach	
Footprint	−225.8 ± 58.9
Mapped	−243.9 ± 21.1
Equal	−220.3 ± 20.7
Eddy covariance	
EC model	−108.7 ± 146.6
Calculated from observations	−140.7

lated with the footprint model over the whole study period. Table 2 also contains the source fractions calculated for eight 45° sectors around the EC mast under neutral atmospheric stability conditions and the total time period during which the wind direction was from each of these sectors. Weighting the source fractions of these eight sectors by wind direction frequency gives another estimate of total contribution from each vegetation type, the "sector" upscaling approach (Table 2). From Figure 3 and Table 2 it is apparent that the source fractions vary considerably during individual half-hour observation periods in response to footprint position and wind direction. However, the variation in calculated footprints and frequency of wind directions is such that over the entire study period the contribution from each vegetation type is very similar to the mapped proportions that, in turn, are very similar to an equal distribution of vegetation types. As a result, therefore, cumulative NEE is similar for all the upscaling approaches at this site during this time period.

[26] It is possible, therefore, even in a situation such as our study site, with as many as six distinct mosaic elements, differing in cumulative NEE by as much as 15 times (GW versus FF; see Table 1) and in the fraction of the study site that they occupy by up to 3 times, that the EC measurements reflect adequately the overall fluxes from heterogeneous landscapes. However, care should be taken in extrapolating this result to other locations characterized by heterogeneous vegetation distribution without recourse to sufficient preliminary micrometeorological characterization of the locality in question. This step is required to ensure adequate representation of the different vegetation types in the observed EC measurements. Here we present a methodology where the use of a vegetation map and prior knowledge of wind direction and frequency allow this to be assessed. A suitably cautious approach such as this should encourage the application of the EC technique to a wider range of realistically heterogeneous situations in the future; such applications are important to provide flux data for the majority of landscapes and ecosystems in which heterogeneity at scales of 10^1–10^2 m frequently is characteristic.

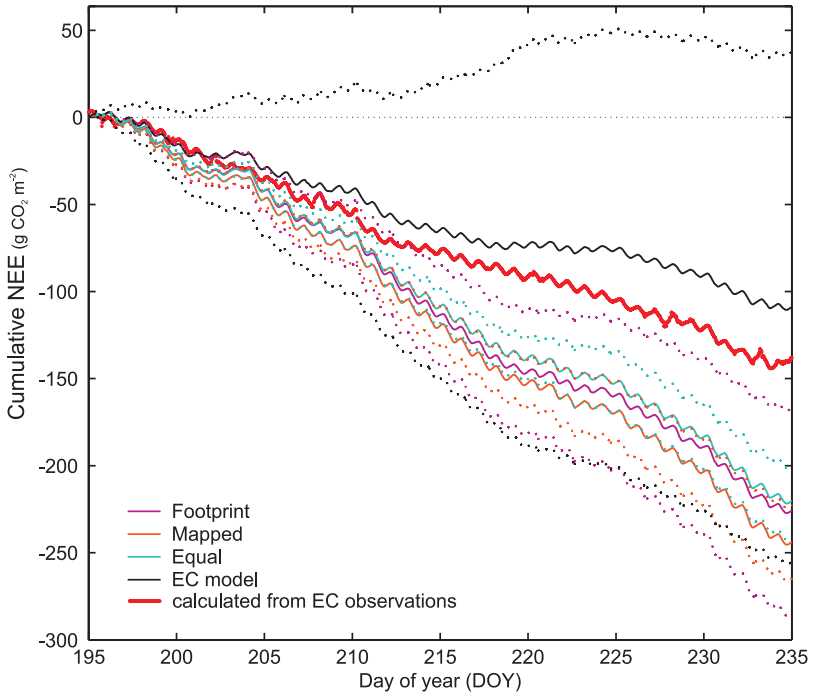

Figure 6. Cumulative upscaled simulated NEE and cumulative observed NEE for the study period. Cumulative NEE (mean, solid lines; ±1 σ^2, dotted lines) for the 40-day study period simulated using three upscaling approaches (see text and Figure 5 for details) and using the PIRT model for the EC data ("EC model"). The cumulative NEE calculated from the gap-filled time series of EC observations is also shown for comparison.

Table 2. Source Fractions and Corresponding Cumulative NEE Over 40-day Study Period for Eight 45° Sectors Around the EC Mast and for Upscaling Approaches

	FF ± 1 σ^2	OE ± 1 σ^2	CE ± 1 σ^2	PF ± 1 σ^2	ST ± 1 σ^2	GW ± 1 σ^2	Time (h)	Cumulative NEE ± 1 σ^2 (g CO_2 m^{-2})
Direction (deg)								
1–45	0.07 ± 0.01	0.19 ± 0.04	0.07 ± 0.04	0.27 ± 0.03	0.38 ± 0.04	0.02 ± 0.01	149.5	−231.3 ± 21.5
46–90	0.02 ± 0.01	0.25 ± 0.03	0.29 ± 0.03	0.14 ± 0.03	0.19 ± 0.03	0.10 ± 0.01	117	−198.4 ± 21.0
91–135	0.11 ± 0.02	0.25 ± 0.03	0.34 ± 0.05	0.08 ± 0.03	0.15 ± 0.03	0.08 ± 0.02	102	−164.2 ± 23.9
136–180	0.08 ± 0.02	0.21 ± 0.03	0.22 ± 0.03	0.25 ± 0.05	0.10 ± 0.03	0.14 ± 0.02	210	−189.6 ± 18.0
181–225	0.04 ± 0.01	0.17 ± 0.02	0.24 ± 0.03	0.16 ± 0.03	0.18 ± 0.05	0.21 ± 0.04	162	−248.9 ± 22.9
226–270	0.07 ± 0.01	0.18 ± 0.02	0.21 ± 0.02	0.04 ± 0.04	0.34 ± 0.10	0.17 ± 0.06	40	−278.1 ± 26.9
271–315	0.04 ± 0.01	0.18 ± 0.02	0.13 ± 0.03	0.15 ± 0.05	0.45 ± 0.09	0.06 ± 0.03	81.5	−269.5 ± 26.9
316–360	0.10 ± 0.01	0.12 ± 0.03	0.04 ± 0.03	0.31 ± 0.03	0.41 ± 0.08	0.02 ± 0.01	98.5	−244.5 ± 21.9
Upscaling approach								
Footprint	0.06 ± 0.01	0.19 ± 0.01	0.21 ± 0.01	0.23 ± 0.01	0.26 ± 0.01	0.11 ± 0.01		−225.8 ± 58.9
Mapped	0.08	0.17	0.21	0.15	0.21	0.18		−243.9 ± 21.1
Equal	0.17	0.17	0.17	0.17	0.17	0.17		−220.3 ± 20.7
Sector	0.07	0.20 ± 0.03	0.19 ± 0.03	0.20 ± 0.04	0.24 ± 0.05	0.10 ± 0.02		−220.7 ± 21.9

[27] Notwithstanding the foregoing, however, our results also lead to the conclusion that there may be significant biases between NEE estimates calculated from EC data and NEE estimates obtained by upscaling from chamber measurements (Figure 6). In the present study the cumulative NEE for the 40-day study period obtained by upscaling chamber measurements was >60% greater in absolute value than the cumulative NEE value calculated from the EC observations. While it is not possible with the available data to determine which value is closer to the "real" NEE, an assessment of the limitations of the two approaches is called for in order to identify potential causes of the observed bias. The EC technique has well-known limitations, for example, in relation to stable atmospheric conditions or to precipitation events during which the open path infrared gas analyzer does not give reliable data and also gives a proportion of outlier or implausible values, for example, strong negative CO_2 fluxes during the hours of darkness. As a result the data obtained must be carefully quality controlled and gap filled in order to obtain acceptable and plausible time series. In the present study, data for >13% of the 1920 half-hour observation intervals were excluded and gap filled, while the FSAM footprint model could be applied only to <30% of the half-hour observation intervals, indicating that the EC data recorded for the majority remainder of these intervals might not conform adequately to the assumptions of the methodology. In addition, previous studies have reported that the EC technique may underestimate fluxes, including CO_2 fluxes, by 10–30% [*Twine et al.*, 2000]. Chamber measurements similarly have a range of limitations, including the limited area and time for which fluxes are sampled and the various ways in which the chambers used modify the conditions experienced by the vegetation within the chamber, notably tending to lead to increases in both relative humidity and temperature. Chamber measurements also are made almost exclusively during the hours of daylight and rarely during or immediately following periods of precipitation.

[28] Given the known limitations of both methods, and the magnitude of the observed bias, it is important to establish and address the causes of this bias in order to obtain more reliable flux estimates. The importance of the bias observed in the present study can be expressed by calculating the impact of such a bias on an estimate of the overall NEE of the tundra regions. The difference in cumulative NEE for the 40-day study period between the footprint upscaled value and the value calculated from the EC observations was ~85 g CO_2 m^{-2} (Table 1). Assuming an average overall growing season length of 75 days for tundra regions, and taking their global extent to be 10.5×10^6 km^2 as given by *Callaghan et al.* [2005], this bias would, if such data were used as a basis to upscale to the entire tundra region, amount to a difference in the annual uptake of carbon by these regions of 0.456 Pg C a^{-1}. To put this figure in perspective, it is almost 8% of the 1990 global fossil fuel emission of carbon to the atmosphere [*IPCC*, 2000]; in terms of a global carbon budget, therefore, a potential bias of this magnitude is of considerable importance. Although such a simplistic approach to upscaling may not be very realistic, these results are nonetheless informative when attempting regional-scale estimates using terrestrial carbon cycle models. In this latter case, field observations may be used for testing model processes, making direct comparisons with model simulations and optimizing model parameter values. However, there is often no explicit consideration of scale in the determination of parameter values. Our multiscale data provide a basis for improving the parameterization process by allowing a better representation of the errors that might occur.

[29] A variety of causes can be hypothesized for this bias. On the one hand, the EC data may be underestimating CO_2 uptake if, for example, the extent of the footprint is systematically exaggerated by the footprint model or uptake rates are greater, all else being equal, during periods with precipitation or of stable atmospheric conditions that prevent collection of meaningful EC data. Although the latter hypothetical possibilities deserve consideration and investigation, they are perhaps less likely to account for the majority of the bias than is a combination of the reported systematic underestimation of the fluxes by the EC technique [*Twine et al.*, 2000] plus the various limitations of the upscaling of fluxes from chamber measurements. A number of hypotheses can be advanced in relation to the latter limitations, including the following. (1) Inherent circadian

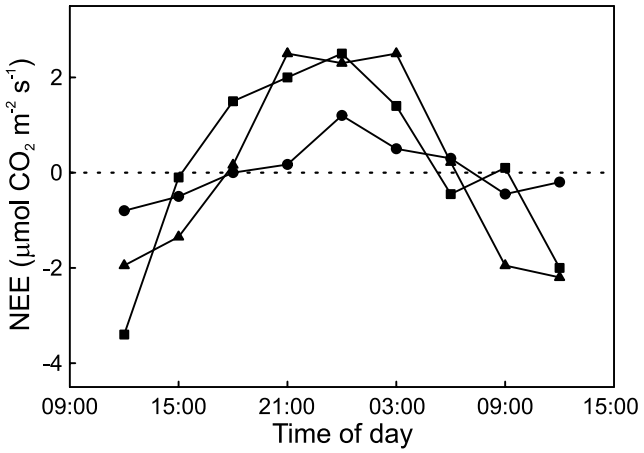

Figure 7. Diurnal pattern of NEE for the CE mosaic element. NEE for the CE mosaic element measured during three 24-h study periods (1200–1200 UT) in 2004. Measurements were made on 2–3 June (circles), 16–17 July (squares), and 25–26 August (triangles).

rhythms of diurnal stomatal closure and/or of other physiological mechanisms may limit or prevent photosynthetic activity during periods of the "nighttime" when PAR levels nonetheless are above the compensation point and the PIRT model fitted to the chamber data thus simulates photosynthesis. (2) Failure to allow for the temperature sensitivity of photosynthesis in the PIRT model may result in higher levels of photosynthesis being simulated, for example, during the early morning hours when PAR is relatively high but temperatures remain relatively cool. (3) Failure to allow for the sensitivity of photosynthesis to VPD in the PIRT model may result in higher levels of photosynthesis being simulated during periods of high VPD when stomatal conductance, and thus actual photosynthesis, is low. (4) Dark chamber measurements used to calibrate the respiration terms in the PIRT model are unrepresentative of the true range of ecosystem nighttime respiration, or nighttime EC observations are biased, possibly because of the relatively complex terrain surrounding the site. (5) The chamber measurements themselves, apart from the limitations discussed above, may not be representative of the mosaic elements they sampled.

[30] The first of these hypotheses can be evaluated in part using data collected in the present study and in part using additional data collected at the site during an earlier study. The PAR data from the observation period show that nighttime light levels were below the compensation point determined from the chamber measurements for the various mosaic elements for several hours per night already at the beginning of the study period, and by the end of the study period nights were becoming fully dark for some time (Figure 2a). Thus, if the bias arises from the first hypothesized cause, then attention must focus upon the evening and early morning periods when light levels may be high enough to lead to simulated uptake when the plants are in fact not photosynthetically active. Data collected during the summer of 2004 for the CE mosaic element during a series of 24-h observation periods [*Cook*, 2005], however, show that, at least for this extensive community, net CO_2 exchange was negative only for the daytime 10–12 h, the community being a net CO_2 source during the nighttime 12–14 h (Figure 7). (CO_2 exchange was measured within a 20 cm diameter chamber (CPY-2 canopy exchange chamber, PP-Systems, Hertfordshire, UK) inserted onto a fixed clear Perspex collar that was sealed to the ground surface using nonhardening "plumber's putty" (Plumber's Mait, Bostik Findley Ltd., Staffordshire, UK) using an infrared gas analyzer (EGM-4, PP-Systems). Measurements were made at 3-h intervals on three occasions, 2–3 June, 16–17 July, and 26–27 August, PAR, temperature, and soil moisture being recorded concurrently with the gas exchange measurements.) This exchange corresponds well to the diurnal pattern of NEE values simulated by the PIRT models (Figure 2b), where again the values are negative only for ~10–12 h of the day on average. It thus seems unlikely that the bias arises from simulation of photosynthetic uptake at times when the plants are inactive as a result of an inherent circadian rhythm.

[31] The second hypothesis also can largely be discounted on the basis of evidence from the present study. In particular, the same PIRT modeling approach was used to construct the EC model from the EC data as was used to construct the models for the mosaic elements. This model, as would be expected, gives simulated NEE that matches the NEE calculated from the EC observations more closely than do the values simulated by the various upscaling approaches that are based upon the models for the mosaic elements (Figure 4). Furthermore, although the EC model has very large uncertainties, which lead to the $\pm 1\ \sigma^2$ range around its mean value for the cumulative NEE encompassing the mean values simulated by all three of the upscaling approaches (Figure 7), its cumulative NEE is smaller in absolute magnitude than that calculated from the EC observations. Were the PIRT model simulations sufficiently sensitive to the effect of temperature on photosynthetic rate to account for the bias between the NEE values simulated by the upscaling approaches and the values calculated from the EC observations, then the NEE value simulated by the EC model would show a similar bias to those seen for the various upscaling approaches that are based upon the PIRT models for the mosaic elements; instead, the EC model cumulative NEE shows a difference of opposite sign to that of the bias. Incidentally, it should be noted that the bias between the cumulative NEE for the study period simulated by the EC model and that simulated by the footprint model is ~38% greater than the bias between the value simulated by the footprint model and the value calculated from the EC observations, although we are unable to determine which EC data–derived estimate of cumulative NEE is closer to "reality."

[32] In the case of the third hypothesis, the residual plots between footprint upscaled NEE and observed NEE show clearly the tendency to overestimate upscaled NEE at high PAR levels (Figure 5b). A possible explanation for this is the failure to incorporate a stomatal conductance term within the PIRT model, inclusion of which would be expected to result in a reduction in photosynthesis during times with both high PAR and high VPD, such a combina-

tion being characteristic of warm, sunny periods that also often are dry. A plot of the same residual values against VPD (Figure 5c) suggests some such underestimation of NEE at higher VPD. However, the number of data points at high VPD are fewer than at high PAR (78 observations in the upper quartile for VPD and 123 observations in the upper quartile for PAR), and the bias over these ranges is less for VPD (mean -1.12 μmol CO_2 m^{-2} s^{-1}) than for PAR (mean -2.06 μmol CO_2 m^{-2} s^{-1}). The problem of overestimation of photosynthesis was greatest between days 210 and 215, as evidenced by the divergence of the cumulative curves in Figure 7 and the time series of upscaled and observed NEE (Figure 4). During this period VPD was high, although not as high as DOY 206, 216, 218, and 219. Chamber measurements were made on DOY 206 and therefore might be considered to be representative of periods with high VPD, and optimizing the PIRT model with measurements made in these conditions might partially offset inadequacies in model treatment of stomatal conductance as it is implicitly included. On days 216, 218, and 219 upscaled NEE is not overestimated to such an extent.

[33] In the case of our fourth hypothesis it is evident from residual plots between footprint upscaled NEE and observed NEE that the model underestimates respiration during the nighttime (PAR < 25 μmol m^{-2} s^{-1}) (Figure 5b). Indeed, the observed bias of $\sim$85 g CO_2 m^{-2} between cumulative observed NEE and footprint upscaled NEE can be partitioned into $\sim$50 g CO_2 m^{-2} because of overestimation of carbon uptake during the day (discussed in section 5) and $\sim$35 g CO_2 m^{-2} because of underestimation of respiration during the nighttime. Consideration of the time series of modeled and observed nighttime fluxes (Figure 4) shows that the model generally estimates the fluxes well but is unable to simulate the sporadic daily maximum respiration values. The simple temperature-dependent nature of the model is not able to reproduce such high temporal variability given the slowly varying air temperature which suggests either inaccuracies within the model formulation or an artificial variability in EC observations due to measurement problems, although these data do not allow us to speculate further on which is the dominant cause.

[34] Overall, it does not appear that either failure to incorporate stomatal conductance into the PIRT model or the model's inability to reproduce the range of nighttime respiration fluxes can fully explain the apparent overestimation of upscaled NEE, although they are possibly part of the explanation on some occasions. This is supported by the adequate performance of the PIRT model as presented here and of closely related model schemes that have been used successfully in tundra environments across a circumpolar range of study sites [*Shaver et al.*, 2007; *Street et al.*, 2007; *Williams et al.*, 2006].

[35] Although we have at present no data with which to test our fifth hypothesis, we note that the locations selected for chamber measurements usually lie near the center of a patch of the mosaic element being sampled and are selected subjectively rather than according to any random or systematic sampling strategy. We also suspect that there may be an operator bias, albeit perhaps unconsciously, toward selecting locations that do not, for example, exhibit obvious evidence of herbivory, have obvious gaps in the vegetation canopy, or include large rocks. There may even be a positive operator bias in favor of selecting areas of the patch that are vigorous and "healthy" in appearance and that consequently have a high leaf area index (LAI). Any such sampling biases would be likely to result in the NEE measured in the chamber being greater in absolute magnitude than the NEE for the patch as a whole at high PAR because an overestimation of mean patch LAI would result in an overestimate of P_{max} (equation (1)) in the optimization step. Were this the case, then using such chamber measurements as the basis for upscaling approaches to estimate NEE of the landscape would almost inevitably result in biased estimates; furthermore, the bias would be toward a more negative NEE at high PAR, as we have found in the present study. This hypothesis is amenable to testing by carrying out series of chamber measurements at randomly or systematically selected locations within patches of the various mosaic elements, including locations within the zones of transition between elements.

[36] Thus, while our results demonstrate the value and robustness of EC data collected from realistically heterogeneous situations, they also highlight the need for more multiscale studies of land surface–atmosphere fluxes in heterogeneous landscapes in order to investigate the principal causes of the uncertainties in the alternative approaches and the biases between the results they provide. Only in this way can more accurate estimates of the "true" fluxes, and hence more accurate overall carbon budgets, be attained.

[37] **Acknowledgments.** This work formed part of the Snow in Tundra Ecosystems: Patterns, Processes, and Scaling Issues (STEPPS) project funded by the Natural Environment Research Council (NERC), NER/A/S/2001/00460, led by R.B. We thank the Royal Swedish Academy and the staff of the Abisko Scientific Research Station for their assistance. We thank Hans Peter Schmid (Department of Geography, Indiana University) for providing the source code for his flux source area model (FSAM). We thank Gus R. Shaver and Lorna E. Street for making available to us the data from their chamber measurements used to model the NEE of the mosaic elements (collected as part of the MBL-ITEX Project supported by NSF grant OPP-03523897); Cath Thompson and Carrie McCalley assisted in the collection of those data. Our gratitude goes also to James G. Cook for making available data from his diurnal series of chamber measurements in the CE mosaic element. Field instrumentation was supported in part through a Royal Society–Wolfson Foundation "Research Merit Award" to B.H. We also thank two anonymous reviewers for constructive comments on a previous version of the paper.

References

Callaghan, T. V., et al. (2005), Arctic tundra and polar desert ecosystems, in *Arctic Climate Impact Assessment*, edited by C. Symon, L. Arris, and B. Heal, pp. 243–352, Cambridge Univ. Press, Cambridge, U. K.

Cook, J. G. (2005), A study on the ecological significance of snow distribution in the low Arctic tundra plant communities of northern Fennoscandia, Ph.D. thesis, Univ. of Durham, Durham, U. K.

Corradi, C., O. Kolle, K. Walter, S. A. Zimov, and E. D. Schulze (2005), Carbon dioxide and methane exchange of a north-east Siberian tussock tundra, *Global Change Biol.*, *11*, 1910–1925.

Cubasch, U., G. A. Meehl, G. J. Boer, R. J. Stouffer, M. Dix, A. Noda, C. A. Senior, S. Raper, and K. S. Yap (2001), Projections of future climate change, in *Climate Change 2001: The Scientific Basis*, edited by J. T. Houghton et al., pp. 525–582, Cambridge Univ. Press, Cambridge, U. K.

Dore, S., G. J. Hymus, D. P. Johnson, C. R. Hinkle, R. Valentini, and B. G. Drake (2003), Cross validation of open-top chamber and eddy covariance measurements of ecosystem CO_2 exchange in a Florida scrub-oak ecosystem, *Global Change Biol.*, *9*, 84–95, doi:10.1046/j.1365-2486.2003.00561.x.

Griffis, T. J., T. A. Black, D. Gaumont-Guay, G. B. Drewitt, Z. Nesic, A. G. Barr, K. Morgenstern, and N. Kljun (2004), Seasonal variation and partitioning of ecosystem respiration in a southern boreal aspen forest, *Agric. For. Meteorol.*, *125*, 207–223, doi:10.1016/j.agrformet.2004.04.006.

Gryning, S. E., A. A. M. Holtslag, J. S. Irwin, and B. Sivertsen (1987), Applied dispersion modeling based on meteorological scaling parameters, *Atmos. Environ.*, *21*, 79–89, doi:10.1016/0004-6981(87)90273-3.

Heikkinen, J. E. P., M. Maljanen, M. Aurela, K. J. Hargreaves, and P. J. Martikainen (2002), Carbon dioxide and methane dynamics in a sub-Arctic peatland in northern Finland, *Polar Res.*, *21*, 49–62, doi:10.1111/j.1751-8369.2002.tb00066.x.

Heikkinen, J. E. P., T. Virtanen, J. T. Huttunen, V. Elsakov, and P. J. Martikainen (2004), Carbon balance in east European tundra, *Global Biogeochem. Cycles*, *18*, GB1023, doi:10.1029/2003GB002054.

Horst, T. W., and J. C. Weil (1992), Footprint estimation for scalar flux measurements in the atmospheric surface layer, *Boundary Layer Meteorol.*, *59*, 279–296, doi:10.1007/BF00119817.

Horst, T. W., and J. C. Weil (1994), How far is far enough?: The fetch requirements for micrometeorological measurement of surface fluxes, *J. Atmos. Oceanic Technol.*, *11*, 1018–1025, doi:10.1175/1520-0426(1994)011<1018:HFIFET>2.0.CO;2.

Intergovernmental Panel on Climate Change (IPCC) (2000), *Special Report on Emissions Scenarios*, edited by N. Nakicenovic and R. Swart, 570 pp., Cambridge Univ. Press, Cambridge, U. K.

Intergovernmental Panel on Climate Change (IPCC) (2001), *Climate Change 2001: Synthesis Report*, edited by R. T. Watson et al., 398 pp., Cambridge Univ. Press, Cambridge, U. K.

Intergovernmental Panel on Climate Change (IPCC) (2007), Summary for policymakers, in *Climate Change 2007: The Physical Science Basis: Working Group I Contribution to the Fourth Assessment Report of the IPCC*, edited by S. Solomon, D. Qin, and M. Manning, pp. 1–18, Cambridge Univ. Press, New York.

Kabwe, L. K., R. E. Farrell, S. K. Carey, M. J. Hendry, and G. W. Wilson (2005), Characterizing spatial and temporal variations in CO_2 fluxes from ground surface using three complimentary measurement techniques, *J. Hydrol.*, *311*, 80–90.

Kennedy, M. C., and A. O'Hagan (2000), Predicting the output from a complex computer code when fast approximations are available, *Biometrika*, *87*, 1–13, doi:10.1093/biomet/87.1.1.

Kennedy, M. C., and A. O'Hagan (2001), Bayesian calibration of computer models, *J. R. Stat. Soc., Ser. B*, *63*, 425–450, doi:10.1111/1467-9868.00294.

Kennedy, M. C., C. W. Anderson, S. Conti, and A. O'Hagan (2006), Case studies in Gaussian process modelling of computer codes, *Reliab. Eng. Syst. Safety*, *91*, 1301–1309.

Kim, J., Q. Guo, D. D. Baldocchi, M. Leclerc, L. Xu, and H. P. Schmid (2006), Upscaling fluxes from tower to landscape: Overlaying flux footprints on high-resolution (IKONOS) images of vegetation cover, *Agric. For. Meteorol.*, *136*, 132–146, doi:10.1016/j.agrformet.2004.11.015.

Laine, A., M. Sottocornola, G. Kiely, K. A. Byrne, D. Wilson, and E. S. Tuittila (2006), Estimating net ecosystem exchange in a patterned ecosystem: Example from blanket bog, *Agric. For. Meteorol.*, *138*, 231–243, doi:10.1016/j.agrformet.2006.05.005.

McGuire, A. D., et al. (2002), Environmental variation, vegetation distribution, carbon dynamics, and water/energy exchange at high latitudes, *J. Veg. Sci.*, *13*, 301–314, doi:10.1658/1100-9233(2002)013[0301:EVVDCD]2.0.CO;2.

Moncrieff, J. B., J. M. Massheder, H. de Bruin, J. Elbers, T. Friborg, B. Heusinkveld, P. Kabat, S. Scott, H. Soegaard, and A. Verhoef (1997), A system to measure surface fluxes of momentum, sensible heat, water vapour and carbon dioxide, *J. Hydrol.*, *188–189*, 589–611, doi:10.1016/S0022-1694(96)03194-0.

Oechel, W. C., G. L. Vourlitis, S. Brooks, T. L. Crawford, and E. Dumas (1998), Intercomparison among chamber, tower, and aircraft net CO2 and energy fluxes measured during the Arctic system science land-atmosphere-ice interactions (ARCSS-LAII) flux study, *J. Geophys. Res.*, *103*, 28,993–29,003, doi:10.1029/1998JD200015.

Reth, S., M. Gockede, and E. Falge (2005), CO_2 efflux from agricultural soils in eastern Germany—Comparison of a closed chamber system with eddy covariance measurements, *Theor. Appl. Climatol.*, *80*, 105–120, doi:10.1007/s00704-004-0094-z.

Schmid, H. P. (1994), Source areas for scalars and scalar fluxes, *Boundary Layer Meteorol.*, *67*, 293–318, doi:10.1007/BF00713146.

Schmid, H. P. (1997), Experimental design for flux measurements: Matching scales of observations and fluxes, *Agric. For. Meteorol.*, *87*, 179–200, doi:10.1016/S0168-1923(97)00011-7.

Schmid, H. P., and C. R. Lloyd (1999), Spatial representativeness and the location bias of flux footprints over inhomogeneous areas, *Agric. For. Meteorol.*, *93*, 195–209, doi:10.1016/S0168-1923(98)00119-1.

Shaver, G. R., L. E. Street, E. B. Rastetter, M. T. van Wijk, and M. Williams (2007), Functional convergence in regulation of net CO_2 flux in heterogeneous tundra landscapes in Alaska and Sweden, *J. Ecol.*, *95*, 802–817, doi:10.1111/j.1365-2745.2007.01259.x.

Sjogersten, S., and P. A. Wookey (2002), Climatic and resource quality controls on soil respiration across a forest-tundra ecotone in Swedish Lapland, *Soil Biol. Biochem.*, *34*, 1633–1646, doi:10.1016/S0038-0717(02)00147-5.

Sjogersten, S., B. L. Turner, N. Mahieu, L. M. Condron, and P. A. Wookey (2003), Soil organic matter biochemistry and potential susceptibility to climatic change across the forest-tundra ecotone in the Fennoscandian mountains, *Global Change Biol.*, *9*, 759–772, doi:10.1046/j.1365-2486.2003.00598.x.

Smith, W. K., R. D. Kelly, J. M. Welker, J. T. Fahnestock, W. A. Reiners, and E. R. Hunt (2003), Leaf-to-aircraft measurements of net CO_2 exchange in a sagebrush steppe ecosystem, *J. Geophys. Res.*, *108*(D3), 4122, doi:10.1029/2002JD002512.

Soegaard, H., C. Nordstroem, T. Friborg, B. U. Hansen, T. R. Christensen, and C. Bay (2000), Trace gas exchange in a high-arctic valley: 3. Integrating and scaling CO_2 fluxes from canopy to landscape using flux data, footprint modeling, and remote sensing, *Global Biogeochem. Cycles*, *14*, 725–744, doi:10.1029/1999GB001137.

Street, L. E., G. R. Shaver, M. Williams, and M. T. van Wijk (2007), What is the relationship between changes in canopy leaf area and changes in photosynthetic CO_2 flux in Arctic ecosystems?, *J. Ecol.*, *95*, 139–150, doi:10.1111/j.1365-2745.2006.01187.x.

Twine, T. E., W. P. Kustas, J. M. Norman, D. R. Cook, P. R. Houser, T. P. Meyers, J. H. Prueger, P. J. Starks, and M. L. Wesely (2000), Correcting eddy-covariance flux underestimates over a grassland, *Agric. For. Meteorol.*, *103*, 279–300, doi:10.1016/S0168-1923(00)00123-4.

Vanulden, A. P. (1978), Simple estimates for vertical diffusion from sources near the ground, *Atmos. Environ.*, *12*, 2125–2129, doi:10.1016/0004-6981(78)90167-1.

van Wijk, M. T., and W. Bouten (2002), Simulating daily and half-hourly fluxes of forest carbon dioxide and water vapor exchange with a simple model of light and water use, *Ecosystems*, *5*, 597–610, doi:10.1007/s10021-002-0155-z.

Vourlitis, G. L., W. C. Oechel, A. Hope, D. Stow, B. Boynton, J. Verfaillie, R. Zulueta, and S. J. Hastings (2000), Physiological models for scaling plot measurements of CO_2 flux across an Arctic tundra landscape, *Ecol. Appl.*, *10*, 60–72.

Williams, M., L. E. Street, M. T. van Wijk, and G. R. Shaver (2006), Identifying differences in carbon exchange among Arctic ecosystem types, *Ecosystems*, *9*, 288–304, doi:10.1007/s10021-005-0146-y.

R. Baxter, A. M. Fox, and B. Huntley, Institute of Ecosystem Science, School of Biological and Biomedical Sciences, University of Durham, South Road, Durham DH1 3LE, UK. (robert.baxter@durham.ac.uk)

C. R. Lloyd, Centre for Ecology and Hydrology, Wallingford OX10 8BB, UK.

M. Williams, Institute of Atmospheric and Environmental Sciences, School of Geosciences, University of Edinburgh, Crew Building, The King's Buildings, West Mains Road, Edinburgh EH9 3JN, UK.